Relationship between the expansion of drylands and the intensification of Hadley circulation during the late 20th century

Sang-Hye Shin[1], Il-Ung Chung[2*], and Hyung-Jin Kim[3]

1: Department of Atmospheric Sciences, Yonsei University, Korea

2: Department of Atmospheric and Environmental Sciences,

Gangneung-Wonju National University, Korea

3: Research Institute for Global Change,

Japan Agency for Marine-Earth Science and Technology, Japan

Meteorology and Atmospheric Physics

Submitted on June 14, 2012

* Corresponding author: Il-Ung Chung
Department of Atmospheric and Environmental Sciences
Gangnung- Wonju National University, Gangneung, Korea
Email: iuchung@gwnu.ac.kr
Phone: 82-33-640-2325
Fax: 82-33-640-2320

Abstract

The changes in coverage by arid climate and intensity of the Hadley circulation during the second half of the 20th century were examined using observations and the multi-model ensemble (MME) mean of Twentieth-Century Coupled Climate Model (20C3M) simulations. It was found that the area of dry climate, which comprises steppe and desert climates following the Köppen climate classification, expanded to an appreciable extent in observation and, to a lesser degree, in MME simulation. The areal extent of steppe climate (the outer boundary of arid climate) tends to encroach on the surrounding climate groups, which, in turn, feeds desert climate (the inner part of arid climate) and causes it to grow. This result indicates the importance of accurate prediction for climate regimes that border steppe climate. Concomitant with the expansion of drylands, the observed intensity of the Hadley cell is persistently enhanced, particularly during boreal winter, suggesting the validity of a self-induction of deserts through a positive bio-geophysical feedback (also known as Charney's cycle). In comparison, the simulated Hadley circulation in the MME mean remains invariant in time. The current climate models, therefore, disagree with the observation in the long-term linkage between desertification and Hadley cell. Finally, the implication of such discrepancy is discussed as a possible guidance to improve models.

Keywords: dryland expansion, Hadley circulation, climate change, 20C3M simulations

1. Introduction

During the 20th century, climate change due to global warming has occurred worldwide. The Intergovernmental Panel on Climate Change Fourth Assessment Report (IPCC AR4, 2007) documented that an increase in anthropogenic greenhouse gas (GHG) causes a rise in global temperature, which, in turn, alters global water cycles through modulation of atmospheric circulation (Held and Soden, 2006). The changing aspects of the hydrological cycle manifest in different ways. The frequency of heavy rainfall, for example, has increased in most continents (Groisman et al., 2005), whereas the Mediterranean, southwestern U.S., and other northern subtropical regions have experienced decreased precipitation in recent decades (Mariotti et al., 2008; Zhang et al., 2007). Dry regions and their rainfall amount also underwent noticeable changes during the late 20th century when rapid global warming progressed, as revealed by the expansion of drylands in subtropical regions (Fraedrich et al., 2001; Beck et al., 2006) and more severe and longer droughts in the tropics and extratropics (IPCC, 2007).

According to the United Nations Convention to Combat Desertification, dryland is defined as land with hyper-arid deserts, arid, semi-arid, and dry sub-humid areas resulting from climate variations and human activities (Reynolds and Smith, 2002). Drylands cover approximately 41.3% of the world's land area, supporting 2 billion people, and up to 44% of all cultivated land is located in drylands. Unsustainable land and water use and climate change are driving the degradation of drylands. About 6 million km^2 (10%) of drylands bear a legacy of land degradation (UN EMG, 2011). Hence, about 250 million people around the world are under the direct influence of land degradation, and about 1 billion people in over 100 countries are at risk (WMO, 2005).

The vulnerability of arid climate regime is often termed as desertification.

Desertification occurs for various reasons, such as natural variability in atmospheric circulation, human-induced soil deterioration (e.g., excessive pasturage and cultivation), deforestation, environmental pollution, and anthropogenic global warming. In the past, it was suggested that the major causes in desertification were overgrazing and excessive cultivation following an increase in population. However, increasing evidence has recently suggested that desert is also fairly susceptible to global warming (Fraedrich et al., 2001; Beck et al., 2006; Kim et al., 2008; Chung and Shin, 2011).

Over drylands, a high albedo results in a net radiative heat loss. Consequently, the overlying air must descend and compress adiabatically in order to maintain thermal equilibrium. These processes explain why most deserts on Earth are formed beneath the subtropical sinking motions of the tropical meridional circulation. Besides, this geographical configuration implies the possible existence of long-term covariability between the Hadley circulation and land degradation in a changing climate. The influence of global warming on desertification via tropical circulation was proposed earlier by Charney (1975). Hitherto, however, few efforts have been made to verify the linkage in spite of the fact that the relationship between changes in Hadley circulation intensity and the warming trend has been extensively investigated (Quan et al., 2004; Tanaka et al., 2004; Song and Zhang, 2007; Takemoto and Tanaka, 2007).

This paper aims to fill this knowledge gap by investigating observational evidences for long-term and inter-decadal relationships between the desertification and intensification of Hadley circulation during the second half of the 20th century. It also assesses the skill of current coupled global climate models (CGCMs) in reproducing such relationships by comparing multi-model simulations with observations. In Section 2, we describe the data and methods used for the analyses. The expansion of drylands

and changes in Hadley circulation intensity are addressed in Section 3 and 4, respectively. Conclusions and discussions are presented in Section 5.

2. Data and methods

2.1 Data

The Program for Climate Model Diagnosis and Intercomparison has archived various simulations submitted by international research centers around the world. Among the collections, monthly means of surface air temperature, precipitation, and horizontal winds at 200-hPa from the Twentieth-Century Coupled Climate Model (20C3M) simulations were analyzed. The twenty-two CGCMs used in this study include CCCMA-T47, CCCMA-T63, CNRM-CM3, CSIRO-MK3.0, CSIRO-MK3.5, GFDL-CM2.0, GFDL-CM2.1, GISS-AOM, GISS-EH, GISS-ER, IAP, INM-CM3.0, IPSL-CM4, MIROC-3.2 (hires), MIROC-3.2 (medres), MIUB, MPI-ECHAM5, MRI-CGCM2.3.2, NCAR-CCSM3.0, NCAR-PCM1, UKMO-HadCM3, and UKMO-HadGEM1. The 20C3M simulations are commonly forced with historical changes in greenhouse gases, but some models additionally include specific forcings, such as sulfate aerosols, volcanic eruptions, and solar forcings (Santer et al., 2006). Detailed descriptions of the individual models are available on-line at http://www-pcmdi.llnl.gov/ipcc/about_ipcc.php. The analysis period for the 20C3M outputs was from 1950 to 1999. Each model's resolution was preserved for analysis of desertification, but for the change of Hadley circulation, all model outputs were interpolated onto a uniform grid system of 2.5°×2.5° by conducting bi-linear interpolation.

For the detection and validation of arid climate change, monthly mean temperature and precipitation were taken from the Climatic Research Unit data set, CRU TS 2.1 (Mitchell and Jones, 2005). This data set spans from 1901 to 2002 and covers the entirety of global land except Antarctica at 0.5°×0.5° resolution. Yet the actual period used is confined to the period of 1950-2000. In case of the Hadley circulation, the ECMWF 40-year reanalysis project (ERA40, Uppala et al., 2005) was employed for 1961-2000 with grid spacing of 2.5°×2.5°.

2.2 Methods

2.2.1 Climate classification

In order to probe whether the evolution of drylands shows a significant signal, an essential prerequisite is a realistic demarcation of various climate regimes. Using a normalized difference vegetation index derived from satellite remote sensing would be a good approach, especially for depicting the area of arid climate (e.g., Piao et al., 2005). However, satellite observations started only from the late 1970s, making it nonfeasible to trace climatic shift on an extended time scale. Instead, a conventional bioclimatic scheme originally proposed by Köppen (1936) was adopted. The Köppen climate classification is a nominal representation of different climate types based on environmental characteristics (e.g., vegetation) (Beck et al., 2005). The main merit of this traditional method is the use of annual-mean near-surface temperatures and annual precipitation sums (referred to as R in the unit of cm in Table 1) that have been recorded for a long time, thereby allowing us to monitor long-term climate change.

Fig. 1 illustrates the thirteen subclasses of the Köppen climate classification over the global land derived from CRU TS 2.1 climatology (1961-1990). The arid regime (B

climate) which is the target of this study, consists of two subclasses, BS (steppe) and BW (desert), defined by the hydrological balance between rain and potential evaporation (see Table 1 for detailed definitions). The criteria used in the Köppen classification are mutually exclusive across the primary and secondary climate types and so is the demarcation of them. Based on Fig. 1, we focused on the areal change and the change in the fractional area of arid climate. Here, *"fractional area"* denotes a ratio of the land area of each climate type to the entire global land area excluding Antarctica.

It should be also mentioned that a well-documented update of the world climate classification has been recently proposed by Kottek et al. (2006). However, its definitions for arid climate are essentially the same as the ones described in Table 1, justifying the generality of the results in the present study.

2.2.2 Intensity of the Hadley circulation

The Hadley cell is a meridional overturning circulation bounded approximately by 30˚S and 30˚N. In the present study, it was derived from the divergent component of horizontal winds following Tanaka et al. (2004) since the three-dimensional structure of atmospheric circulation is strongly influenced by divergent circulation despite the dominant role of rotational (nondivergent) winds in shaping the background structure (Trenberth et al., 2000). Tanaka et al. (2004) calculated velocity potential at 200-hPa and decomposed it into three components generated by the different driving forces. To this end, a zonal mean component is obtained to represent the Hadley circulation driven by the differential meridional heating of the global radiative process. Next, the deviation from the zonal mean is divided further into two components: 1) seasonally changing component, which reflects monsoon circulation driven by land-sea thermal contrast, and

2) the rest of the annual mean component, which is defined as the Walker circulation driven by the sea surface temperature (SST) gradient along the equatorial tropics. By this separation, Tanaka et al. (2004, 2005) demonstrated that the intensities of the different tropical circulations can be effectively quantified to explore their variability on time scales from inter-annual to centennial. The following is a brief description of the mathematical manipulation proposed by Tanaka et al. (2004).

The horizontal wind vector can be expressed by the sum of a non-divergent (or rotational) part and a divergent (or irrotational) part (Krishnamurti, 1971):

$$\vec{V} = \overrightarrow{V_\Psi} + \overrightarrow{V_\chi} = \vec{k} \times \vec{\nabla}\Psi + (-\nabla\chi) \quad (1)$$

where Ψ is stream function and χ is velocity potential. Then the divergence (D), calculated in the spectral domain by means of the spherical harmonic expansion of the horizontal wind vector, is used to solve the Poisson equation:

$$D = \vec{\nabla} \bullet \vec{V} = -\nabla^2\chi \quad (2)$$

This methodology was applied to 200-hPa winds as this level contains information regarding the overall intensity of the tropical circulations (Trenberth et al., 2000; Tanaka et al., 2004). Finally, the Hadley circulation was delineated by zonal mean of χ since it is an axisymmetric part of the circulation driven by meridional differential heating. Once the Hadley cell was derived, the peak value of downward branch was examined to detect the trend of the Hadley cell intensity.

3. The change of dryland area

Prior to the investigation of desertification during the second half of the 20th century, we first analyzed the climatological aspects of arid climate from the CRU TS

2.1 and the 20C3M outputs. Fig. 2 presents the fractional areas estimated for arid climate (B) and its subclasses (BS and BW). In observation, about one-third of the global land area was identified as arid region, and the desert and steppe climate types account for 65 % and 35 % of the total dry area, respectively. The global arid climate in individual model simulations showed a notable spread among models. Two-thirds of the models simulated the area of drylands within $\pm 1\sigma$ levels, and all models except csiro-mk35 simulated it within $\pm 2\sigma$ levels. Nonetheless, the multi-model ensemble (MME) results were fairly comparable to their observed counterparts with relative errors limited to within ±10%. As such, the MME mean was used to assess the fidelity of the model simulations in reproducing the trends and inter-decadal variability.

Fig. 3 shows the observed inter-decadal variations of fractional area (black dots) for the primary and secondary types of dry climate. Apparently, the inter-decadal fluctuations of B climate are determined by BW climate (Figs. 3a and 3c), because the coverage of BW far exceeds that of BS. On the other hand, the increasing trend of arid climate is controlled by BS climate (Figs. 3a and 3b). The statistical significance of the trends was tested by a parametric linear trend test (Wilks, 2006) and a non-parametric Mann-Kendall rank statistics (Kendall, 1955) with effective degree of freedom (EDOF) to take into account the effects of autocorrelation of each time series. For the Mann-Kendall statistics, the EDOF was estimated following Hamed and Rao (1998), in which the autocorrelation function of the ranks of the original data is used to reflect the reduction of degree of freedom. For the linear trend test, on the other hand, it is approximated as N/τ, where N is the number of original data and τ is the de-correlation time scale defined as the time lag of the first zero crossing of the autocorrelation function calculated from the residual data sets. The results showed that although the

EDOFs were decreased notably (ranging from 5 to 6), the trends are significant with the confidence level higher than 99% (90%) by the linear trend test (Mann-Kendall rank statistics). It is also worth noting that the two subtypes share an out-of-phase relationship on the inter-decadal time scale with a correlation coefficient of -0.70 after detrending (Figs. 3b and 3c). This indicates that the retreat (expansion) of the semiarid regime is accompanied by the expansion (retreat) of the desert climate, which is also seen in continental-scale desertification (Kim et al., 2008). The upward trends in B and BS climate turned out to be more substantial over the second half of the 20th century. Chung and Shin (2011) assessed the centennial trend of B (BS) climate during the entire 20th century as 0.06 (0.72) %; about one order of magnitude smaller than the trends during 1951-2000, as shown in Fig. 3. With overall weakening of the trend, the decadal changes of drylands in the MME mean are remarkably suppressed (Fig. 4). Nevertheless, the fractional area of B climate still displays an appreciable increment. Note, however, that the increasing trend is largely attributable to the upward trend in BW. These MME mean trends with the EDOF are also significant with the confidence level higher than 99% (90%) by the linear trend test (Mann-Kendall rank statistics) except that the trend in the BW climate is marginal when the Mann-Kendall rank statistics was applied (about 88% confidence level). The inter-decadal changes of BS and BW climate are weakly correlated with a correlation coefficient of -0.40, which is different from the observational evidence.

Here, the question arises which climate types are the main contributors to the change in the areal extent of arid climate. To answer this question, we investigated the individual contributions from major climate types to arid climate. Table 2 summarizes the area differences between 1981-2000 and 1961-1980. In observation, the increase of

BS climate ($3{,}307\times10^3$ km^2) was accompanied by a reduction in the various climate regimes that surround BS type. Meanwhile, the increase of BW type ($1{,}413\times10^3$ km^2) can be explained predominantly by a decline in steppe climate, because BW borders only BS except in regions with high elevation (Fig. 1). Note also that a transition in the opposite direction (i.e., from BW to BS) is an important source for the expansion of the BS regime. The results from the MME mean bear reasonable resemblance to the observations, though the expansion of steppe (desert) climate was underestimated by about 45 (24) %.

4. The change of the Hadley cell intensity

An increased dryland area in association with the intensification of the Hadley circulation has been reported in previous studies. Chen et al. (2002) reported that the enhanced tropical circulation in the 1990s was related to dryness near the equator and in the subtropical subsidence zone. Hu and Fu (2007) found a poleward movement of the subtropical dry region due to the poleward expansion of the subtropical subsidence zone. In this section, therefore, the decadal change of the Hadley circulation will be discussed with a particular focus on its relationship with the expansion of dry climate area.

Fig. 5 displays the zonal and climatological mean of velocity potential at 200-hPa from December-February (DJF) and June-August (JJA) for the period 1970-1999. Here, a positive (negative) value indicates a divergence and updraft (convergence and downdraft) in the upper troposphere. The MME mean realistically captures the climatological intensities and locations of the Hadley circulations between 30˚S and 30˚N in both hemispheres. But the simulated intensities are obviously reduced

especially in boreal summer season.

The decadal variations of zonally-averaged velocity potential are plotted in Fig. 6. In the ERA40 (upper panels), a gradual increase of the Hadley cell intensity is notable during boreal winter for 1961-2000. Such a tendency, however, becomes vague in JJA. Together, these results could indicate the dynamical influence on the expansion of dry regions, especially the effect of DJF Hadley cell intensification on a monotonic increase in BS climate (marked by black dots in Fig. 3b). The deepening of the Hadley circulation agrees with results discussed in many previous studies (e.g., Tanaka et al., 2004; Mitas and Clement, 2005; Song and Zhang, 2007; Takemoto and Tanaka, 2007). In comparison, the observational consistency between desertification and amplification of the Hadley cell seems to be invalid for the MME mean (lower panels), in which the intensity of the Hadley circulation remains nearly invariant during the second half of the 20^{th} century.

To further investigate the changing trend of Hadley circulation intensity, we looked into the interannual variability of intensity in NH boreal wintertime (DJF) for ERA40 and 20C3M MME mean (Fig. 7). In these graphs, downward (upward) trends represent the strengthening (weakening) of the Hadley circulation. In ERA40, the Hadley circulation became steadily strengthened in the late 20^{th} century with the 99% confidence level. In contrast, the Hadley cell trend in MME mean is virtually flat with reduced year-to-year variability due to multi-model averaging process. The phases of the interannual variability of the simulated Hadley cell differ substantially from one model to another, and hence the MME variability is considerably smoothed out through average process although individual CGCMs' variability is as large as the observed. The observed trends continue for an extended period from November to April, but neither

the MME mean nor the individual models faithfully reproduce the downward trends (Table 3). This discrepancy of the current CGCMs, that is a problematic representation of the long-term trends in spite of reasonably realistic skill in simulating mean states and variability, was also argued by Shin and Sardeshmukh (2011).

It is important to clarify the robustness of the Hadley cell trend found in the ERA40 reanalysis. The trend might be an artifact because reanalysis data sets have an inhomogeneity problem due to changes in the observing system, such as the introduction of satellite data from around 1979. Sterl (2004) emphasized that deep care has to be taken not to confuse the inhomogeneities with real changes when the reanalysis data are used to investigate climate change issues. We argue that the long-term changes of the Hadley circulation intensity are most likely a signal. First, we noticed that the increasing trends exist not only for the whole period (Fig. 7a) but also prior to and after satellite era separately (Fig. 6a). Indeed, the DJF trend after satellite era (1980-2000) is significant at the 90% confidence level or higher with a slope of $-2.96\times10^{5}\ m^{2}s^{-1}dec^{-1}$. Second, Song and Zhang (2007) showed the similar results using NCEP-NCAR reanalysis (Kalnay et al., 1996) over 1948-2006. We also examined the more recent reanalysis of ERA-Interim data (Dee et al., 2011) and result indicates a statistically significant intensification ($-3.99\times10^{5}m^{2}s^{-1}dec^{-1}$) of the DJF Hadley cell during 1990-2010, which is also associated with the decreasing trend ($-3.03Wm^{2}dec^{-1}$) in outgoing longwave radiation over the updraft zone of the Hadley cell (10-20^{o}S) detected from Clouds and the Earth's Radiant Energy System Energy Balanced and Filled dataset (Wielicki et al., 1996).

5. Conclusions

This study investigated the expansion of drylands and related changes of the Hadley circulation during the late 20th century based on analyses of observational data (CRU TS 2.1 dataset and ECMWF 40-year reanalysis) and the 20C3M simulations. A consistent result emerging from the CRU TS 2.1 is the apparent expansion in drylands since 1950. The arid and steppe climate (B and BS type) in the 1990s have expanded outwards by about 1.5% point from those in 1950s (Fig. 3). The desert climate (BW type), on the other hand, appeared to be stable; no distinctive trend in coverage was detected. The 20C3M MME mean also represented the increasing trend of dryland area; yet the magnitude of the increase was considerably small (about 0.3% point), and unlike the observation, the increasing trend of B climate was largely attributable to the trend in BW climate (Fig. 4).

To investigate the key contributors to the change in the areal extent of arid climate, we examined the areal difference between the 1981-2000 and 1961-1980. The areal increase in BS type is due to transition from various climate regimes that surround BS type, whereas in BW climate, the expansion is explained mostly by the conversion from BS climate (98.9% for the observation, and 99.0% for the 20C3M MME). This implies that the BW climate, though stable at present, could expand irreversibly depending upon the extent to which BS climate grows outwards.

In search of dynamical cause of desertification, we also probed the change of the Hadley circulation during the late 20th century. Observational evidences showed that the intensity of the NH winter Hadley circulation has progressively increased since the 1960s, associated with global warming. Such a strengthening is in concert with the gradual expansion of steppe (BS) climate that demarcates the border of B climate and provides a primary source for the increasing trend of B climate. These results are in line

with the traditional notion of desert instability (Charney, 1975), whereby initial land degradation enhances subtropical decent and leads to desertification.

The 20C3M simulations show a minor, but monotonic expansion of dry climate area; however, the amplification of the boreal winter Hadley circulation was simply insignificant. While the observed magnitude (in $10^5 m^2 s^{-1}$) of the boreal winter Hadley circulation intensity increased from -34.7 in the 1960s to -47.9 in the 1990s, the simulated intensity was very stable near the magnitude of -40 for the period from the 1950s to the 1990s. Nevertheless, the desert area of BW climate had persistently increased since 1950. The lack of reality in the model simulations suggests that an interactive coupling between the biosphere and overlying atmosphere, which is beyond the capability of the models examined in the present study, could play a key role on the bio-geophysical feedback of desertification.

We found an observational linkage that connects desertification with intensification of Hadley circulation, and that the current CGCMs had a difficulty to capture it. Particularly in the 21st century, when more rapid and apparent global warming is projected (IPCC, 2007), the change of dryland would be much greater (e.g., Kalvová et al., 2003), and the Hadley circulation would be widened poleward, causing a poleward expansion of the subtropical dry zone (Lu et al., 2007). Furthermore, Zeng and Yoon (2009) found that the world's desert area increased by 10% by considering vegetation-albedo feedbacks in a coupled atmosphere-ocean-land model. These results suggest that unrealistic representations of the arid climate area and the change of the Hadley circulation intensity diagnosed from the 20C3M simulations will be more problematic for the projection of the 21st century climate. Therefore, further studies are necessary for a more reliable assessment, especially with the aid of the state-of-the-art

climate system models with faithful representation of biophysical processes such as vegetation-albedo feedback.

Acknowledgements. We thank the anonymous reviewers for their valuable suggestions. We also acknowledge the modeling groups for making their simulations available for analysis, the Program for Climate Model Diagnosis and Intercomparison for collecting and archiving the CMIP3 model output, and the WCRP's Working Group on Coupled Modelling (WGCM) for organizing the model data analysis activity. The WCRP CMIP3 multimodel dataset is supported by the Office of Science, U.S. Department of Energy.

This work was performed under the auspices of National Institute of Meteorological Research, Korea. H.-J. Kim was supported by the Ministry of the Environment, Japan, under the Environment Research & Technology Development Fund (A0902).

References

Beck C, Grieser J, Kottek M, Rubel F, Rudolf B (2006) Characterizing global climate change by means of Köppen climate classification. DWD, Klimastatusbericht 2005, Deutscher Wetterdienst, ISBN 3-88148-413-2.

Charney JG (1975) Dynamics of deserts and drought in Sahel. Quart J Roy Meteor Soc 101:193-202.

Chung I-U, Shin S-H (2011) Observed change of climatic regions and desertification during the 20th century. Climate Research 6:23-44 (in Korean).

Dee DP et al. (2011) The ERA-Interim reanalysis: configuration and performance of the

data assimilation system. Quart J Roy Meteor Soc 137:553-597.

Fraedrich K, Gerstengarbe FW, Werner PC (2001) Climate shifts in the last century. Climatic Change 50:405-417.

Groisman PYa et al. (2005) Trends in intense precipitation in the climate record. J Climate 18:1326-1350.

Hamed KH, Rao AR (1998) A modified Mann-Kendall trend test for autocorrelated data. J Hydrol 204:182–196.

Held IM, Soden BJ (2006) Robust responses of the hydrological cycle to global warming. J Climate 19:5686-5699.

IPCC (2007) Climate Change 2007: The Physical Science Basis. Contributing of Working Group I to the Fourth Assessment Report of the Intergovernmental Panel on Climate Change [Solomon, S., Quin, D., Manning, M., Chen, Z., Marquis, M., Averyt, K. B., Tignor, M., Miller, H. L. (eds.)]. Cambridge University Press, Cambridge, United Kingdom and New York, NY, USA, 996 pp.

Kalnay E et al. (1996) The NCEP/NCAR 40-year Reanalysis Project. Bull Amer Meteor Soc 77:437-471.

Kalvová J, Halenka T, Bezpalcová K, Nemešová I (2003) Köppen climate types in observed and simulated climates. Stud Geophys Geod 47:185–202.

Kendall MG (1955) Rank correlation Methods. Oxford University Press. New York. 196pp.

Kim H-J, Wang B, Ding Q, Chung I-U (2008) Changes in arid climate over North China detected by the Köppen climate classification. J Meteor Soc Japan 86:981-990.

Köppen W (1936) Das geographische System der Klimate(Handhunch der Klimatologie,

Bd, 1, Teil C).

Kottek M, Grieser J, Beck C, Rudolf B, Rubel F (2006) World map of the Köppen-Geiger climate classification updated. Meteorol Z 15:259-263.

Krishnamurti TN (1971) Tropical east-west circulations during the northern summer. J Atmos Sci 28:1342-1347.

Lu J, Vecchi GA, Reichler T (2007) Expansion of the Hadley cell under global warming. Geophys Res Lett, 34, L06805, doi:10.1029/2006GL028443.

Mariotti A et al. (2008) Mediterranean water cycle change: Transition to drier 21st century conditions in observation and CMIP3 simulations. Environ Res Lett 3:044001.

Mitas CM, Clemente A (2005) Has the Hadley cell been strengthening in recent decades? Geophys Res Lett, 32, L03809, doi:10.1029/2004GL021765.

Mitchell T, Jones P (2005) An improved method of constructing a database of monthly climate observations and associated high-resolution grids. Int J Climatol 25:693-712.

Piao S, Fang J, Liu H, Zhu B (2005) NDVI indicated decline in desertification in China in the past two decades. Geophys Res Lett, 32, L06402, doi:10.1029/2004GL021764.

Quan X-W, Diaz HF, Hoerling MP (2004) Change of the Hadley circulation since 1950. The Hadley Circulation: Past, Present, and Future edited by H.F. Diaz and R.S. Bradley, Kluwer Academic Publishers, 85-120.

Reynolds JF, Smith SM (2002) Global Desertification: Do humans cause deserts? Dahlem University Press, Berlin, 1-22.

Santer BD et al. (2000) Interpreting differential temperature trends at the surface and the

lower troposphere. Science 287:1227-1231.

Shin SI, Sardeshmukh PD (2011) Critical influence of the pattern of tropical ocean warming on remote climate trends. Clim Dyn 36:1577-1591.

Song H, Zhang M (2007) Changes of the boreal winter Hadley circulation in the NCEP-NCAR and ECMWF reanalyses: A comprehensive study. J Climate 20:5191-5200.

Sterl A (2004) On the (in)homogeneity of reanalysis products. J Climate 17:3866-3873.

Takemoto M, Tanaka HL (2007) Intensities of Hadley, Walker, and monsoon circulations compared in the upper and lower troposphere. Asia-Pacific J Atmos Sci 43:239-251.

Tanaka HL, Ishizaki N, Kitho A (2004) Trend and interannual variability of Walker, monsoon and Hadley circulations defined by velocity potential in the upper troposphere. Tellus 56A:250-269.

Tanaka HL, Ishizaki N, Nohara D (2005) Intercomparison of the intensities and trends of Hadley, Walker, and monsoon circulations in the global warming projections. Sci Online Lett Atmos 1:77-80.

Trenberth KE, Stepaniak DP, Caron JM (2000) The global monsoon as seen through the divergent atmospheric circulation. J Climate 13:3969– 3993.

UN EMG (2011) Global Drylands: A UN system-wide response. United Nations Environment Management Group, 131pp.

Uppala SM et al. (2005) The ERA-40 Reanalysis. Quart J Roy Meteor Soc 131:2961-3012.

Wielicki BA et al. (1996) Clouds and the Earth's Radiant Energy System (CERES): An Earth Observing System Experiment. Bull Amer Meteor Soc 77:853-868.

Wilks DS (2006) Statistical Methods in the Atmospheric Sciences. Academic Press, New York, 627pp.

WMO (2005) Climate and Land Degradation. Report No 989, Geneva, Switzerland, 32pp.

Zeng N, Yoon J (2009) Expansion of the world's deserts due to vegetation-albedo feedback under global warming. Geophys Res Lett, 36, L17401, doi:10.1029/2009GL03699.

Zhang XB et al. (2007) Detection of human influence on twentieth century precipitation trends. Nature 448:461-464.

Figure captions

Fig. 1 Global distribution of the 13 climate types defined by the Köppen climate classification. The 30-year climatology (1961-1990) of the CRU TS 2.1.

Fig. 2 Fractional Area (%) of (a) B (dry), (b) BS (steppe), and (c) BW (desert) climate types for the period of 1961-1990. The gray bars represent CRU TS 2.1 data and multi-model ensemble means, with red bars for each individual 20C3M CGCM simulation and blue lines are $\pm 1\sigma$ levels.

Fig. 3 The decadal variations of fractional area (black dots, in %) relative to the global land area excluding Antarctica for each dry climate type in CRU TS 2.1 Also shown are the result from ten-year moving average (black line) and its linear trend (red line).

Fig. 4 Same as Fig. 3 except for the MME mean of 20C3M simulations.

Fig. 5 Zonal mean of the velocity potential at 200-hPa in (a) DJF and (b) JJA for the period 1970-1999, defined as a measure of the Hadley circulation intensity. The black and red line is ERA40 data, and the 20C3M MME, respectively. The units are $10^5 m^2 s^{-1}$.

Fig. 6 Decadal variations of zonal mean velocity potential at 200-hPa in (a) DJF and (b) JJA of ERA40 for the 1961-2000 (upper panels). Same in (c) DJF and (d) JJA of 20C3M MME for the period 1950-1999 (lower panels).

Fig. 7 Interannual variabilities of DJF Hadley cell intensities (in$10^5 m^2 s^{-1}$) in the late 20^{th} century in (a) ERA40 and (b) 20C3M MME mean (red line) along with the individual model results (gray lines). Green and dotted lines are the linear trend and its 99% confidence levels, respectively.

Table captions

Table 1. Definitions for dry climate zone and types of Köppen climate classification.

Table 2. Transfers into BS and BW climate types from 6 Köppen climate types during 1981-2000 relative to the period of 1961-1980.

Table 3. The trends in the interannual variabilities of boreal winter Hadley cell intensities in ERA40, 20C3M MME, and individual models (unit: $10^5 m^2 s^{-1}$/year).

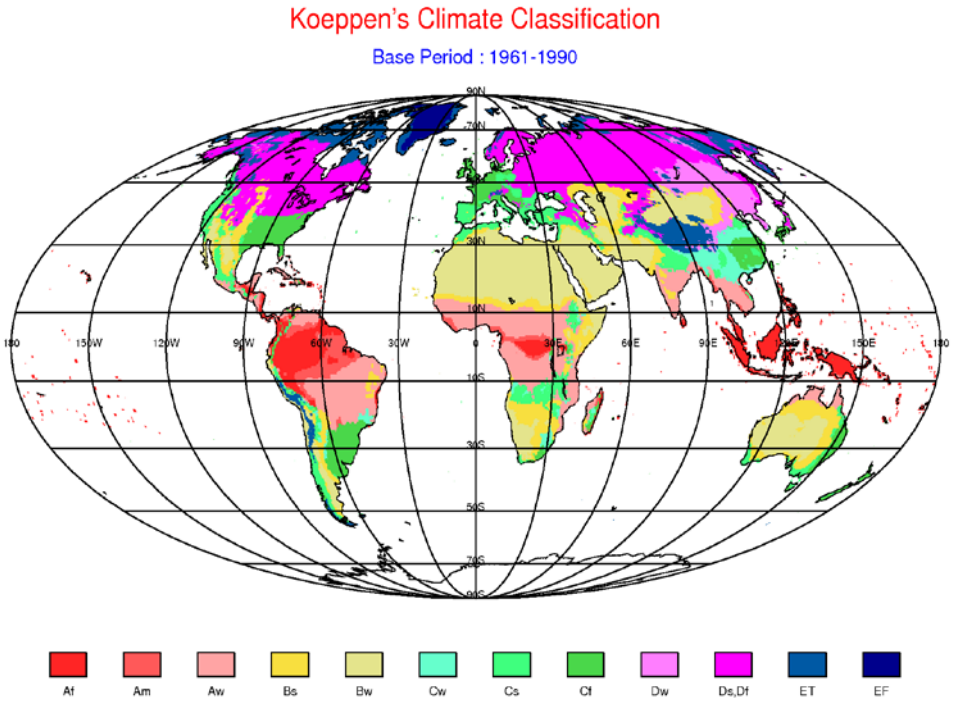
Koeppen's Climate Classification
Base Period : 1961-1990
Af
Am
Aw
Bs
Bw
Cw
Cs
Cf
Dw
Ds,Df
ET
EF

Fig. 1

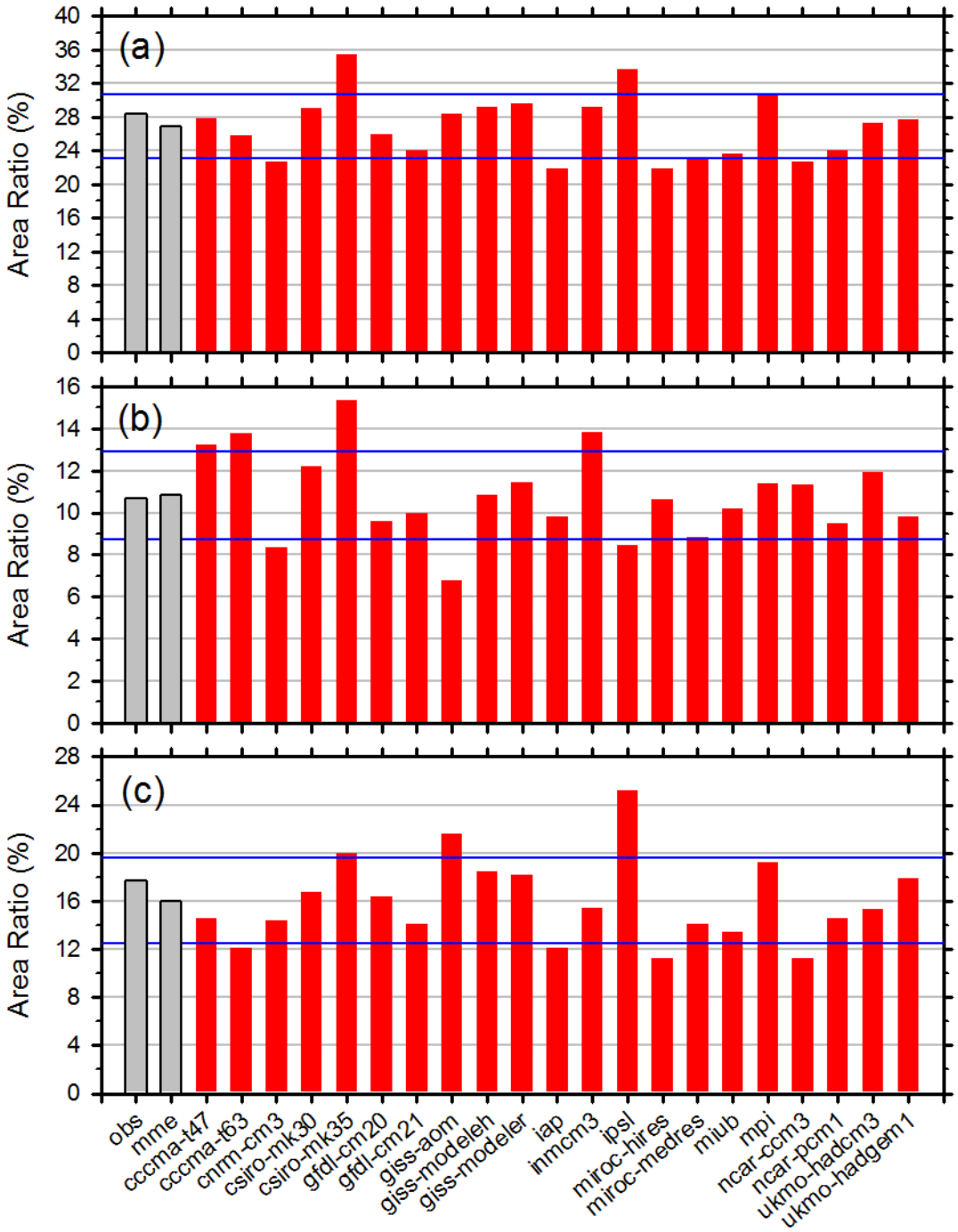
(a)
(b)
(c)
Area Ratio (%)
obs
mme
cccma-t47
cccma-t63
cnrm-cm3
csiro-mk30
csiro-mk35
gfdl-cm20
gfdl-cm21
giss-aom
giss-modeleh
giss-modeler
iap
inmcm3
ipsl
miroc-hires
miroc-medres
miub
mpi
ncar-ccm3
ncar-pcm1
ukmo-hadcm3
ukmo-hadgem1

Fig. 2

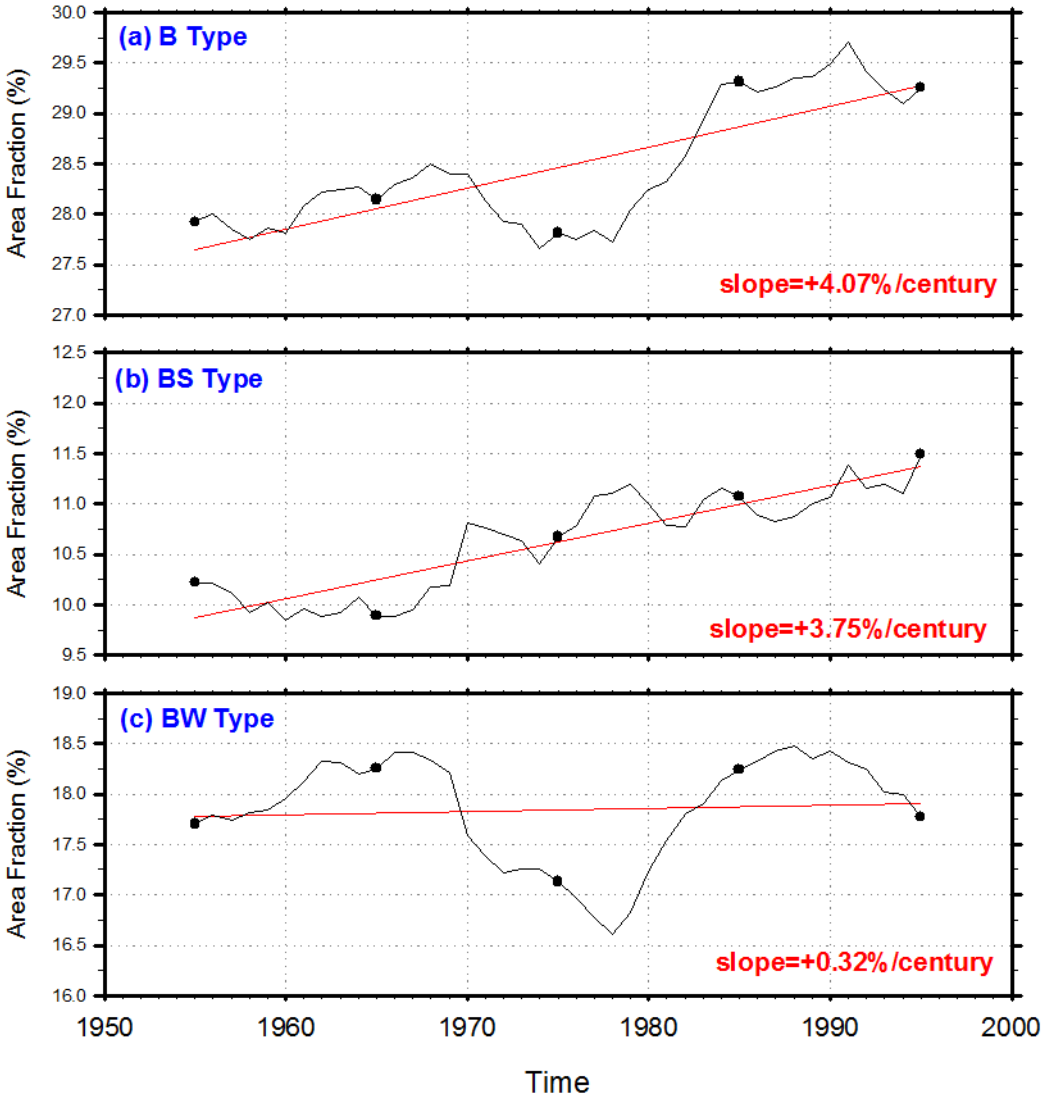
(a) B Type
slope=+4.07%/century
(b) BS Type
slope=+3.75%/century
(c) BW Type
slope=+0.32%/century
Area Fraction (%)
Time
30.0
29.5
29.0
28.5
28.0
27.5
27.0
12.5
12.0
11.5
11.0
10.5
10.0
9.5
19.0
18.5
18.0
17.5
17.0
16.5
16.0
1950
1960
1970
1980
1990
2000

Fig. 3

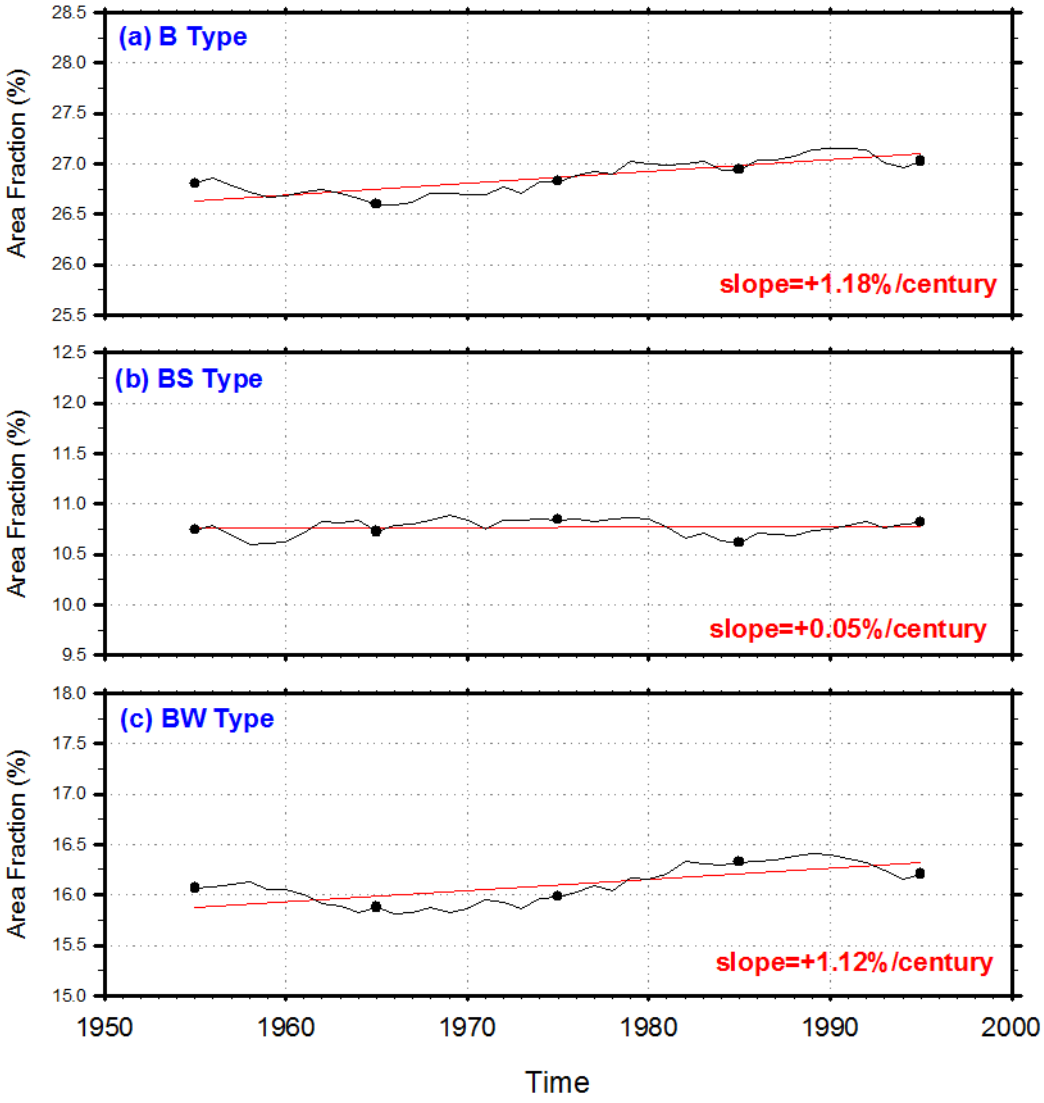
(a) B Type
slope=+1.18%/century
(b) BS Type
slope=+0.05%/century
(c) BW Type
slope=+1.12%/century
Area Fraction (%)
Time
28.5
28.0
27.5
27.0
26.5
26.0
25.5
12.5
12.0
11.5
11.0
10.5
10.0
9.5
18.0
17.5
17.0
16.5
16.0
15.5
15.0
1950
1960
1970
1980
1990
2000

Fig. 4

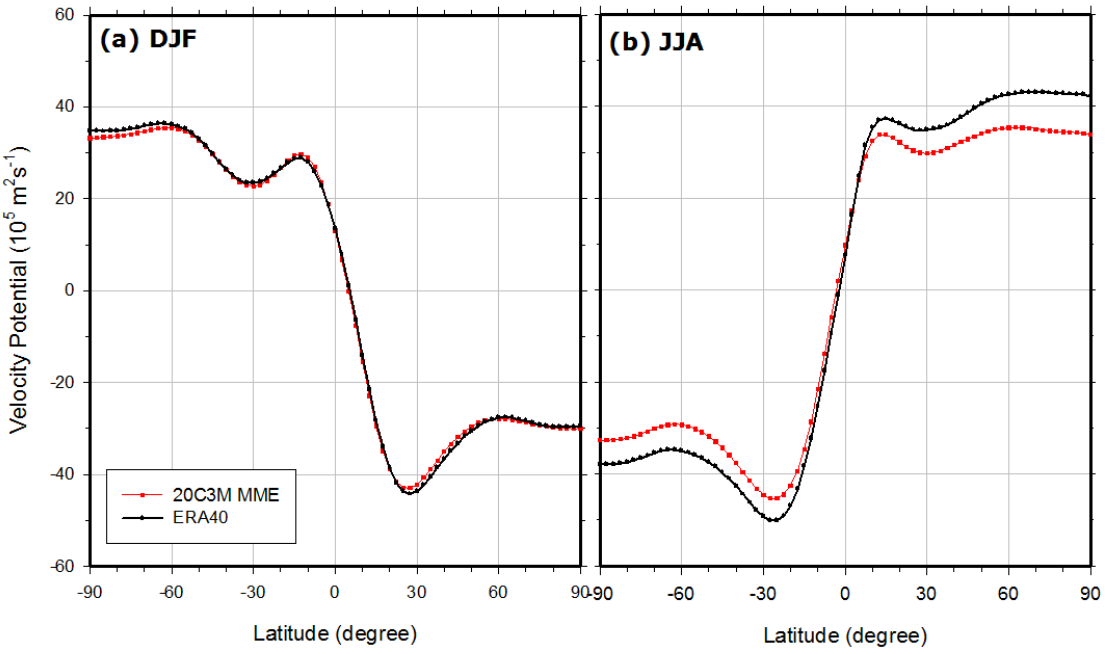
(a) DJF
(b) JJA
Velocity Potential (10^5 m^2s^{-1})
60
40
20
0
-20
-40
-60
-90
-60
-30
0
30
60
90
Latitude (degree)
20C3M MME
ERA40

Fig. 5

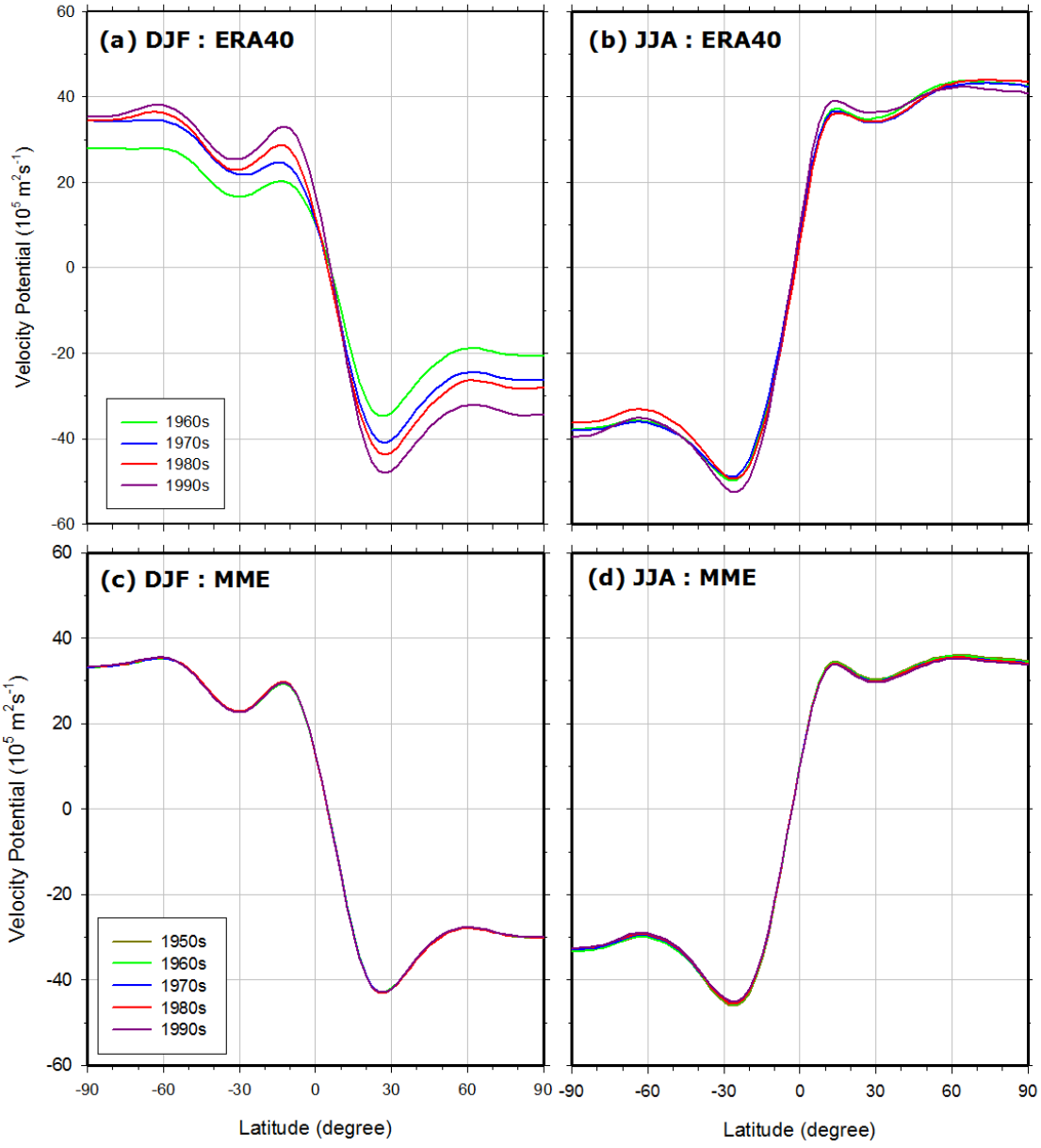
(a) DJF : ERA40
(b) JJA : ERA40
(c) DJF : MME
(d) JJA : MME
Velocity Potential (10^5 m^2s^{-1})
Latitude (degree)
1950s
1960s
1970s
1980s
1990s

Fig. 6

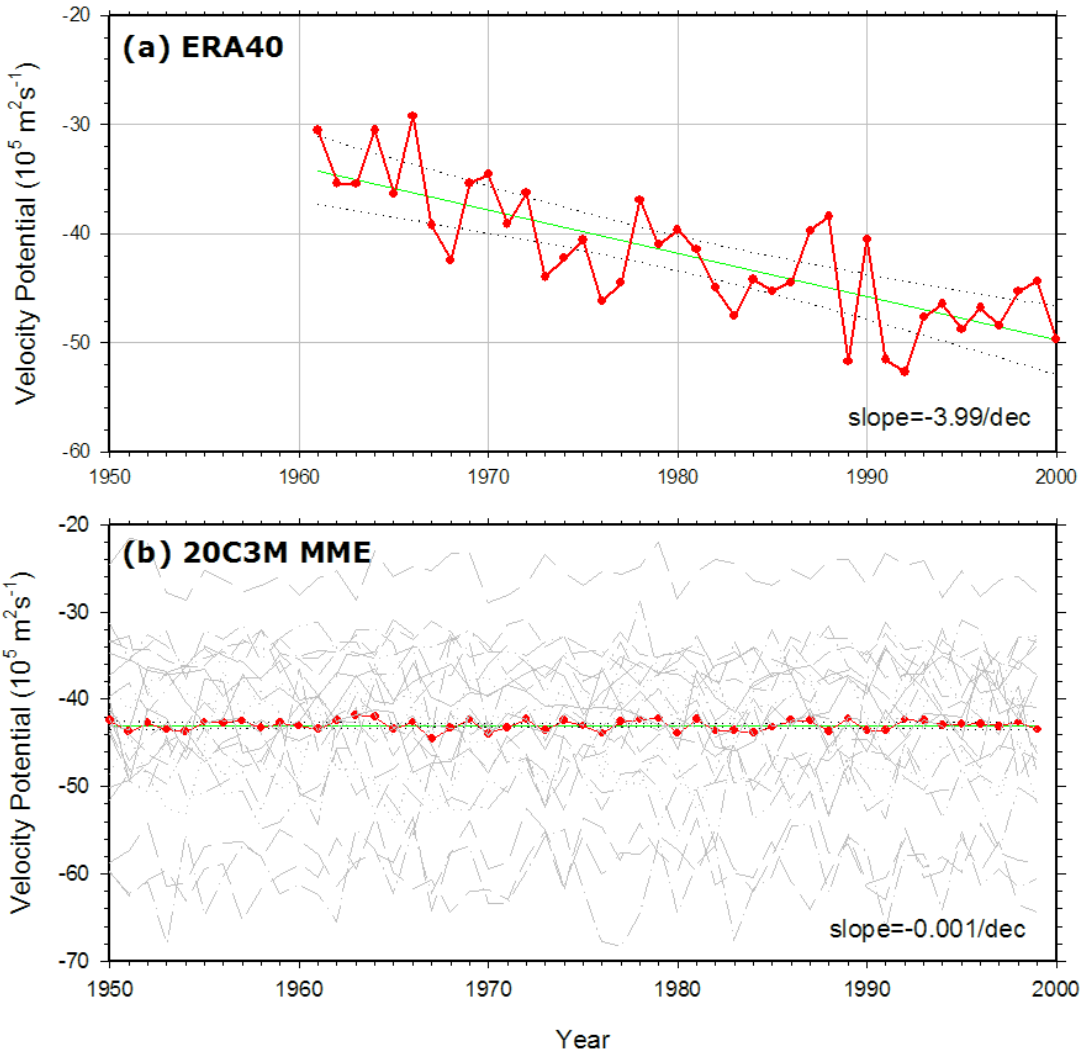
(a) ERA40
Velocity Potential (10^5 m^2s^{-1})
slope=-3.99/dec
(b) 20C3M MME
slope=-0.001/dec
Year

Fig. 7

Table 1.

Major type	Subtype	Definition
B (dry)		▪ Potential evaporation and transpiration exceed precipitation. ▪ R<2T+28 (where 70% or more of annual precipitation falls in the summer half of the year) ▪ R<2T (where 70% or more of annual precipitation falls in the winter half of the year) ▪ R<2T+14 (where neither half of the year has 70% or more of annual precipitation)
	BS (steppe)	annual precipitation is less than the threshold but more than one-half of the threshold
	BW (desert)	annual precipitation is less than one-half of the threshold

Table 2.

From \ To	CRU TS 2.1		MME	
	BS	BW	BS	BW
A (tropical)	22.6%	0.0	17.5%	0.0
BS (steppe)	-	98.9%	-	99.0%
BW (desert)	28.1%	-	29.5%	-
C (temperate)	29.7%	0.0	41.1%	0.0
D (boreal)	19.3%	0.0	11.8%	0.7%
E (cold)	0.3%	1.1%	0.1%	0.3%
Total Areal Change (km^2)	$3{,}307.7\times10^3$	$1{,}413.9\times10^3$	$1{,}817.4\times10^3$	$1{,}069.2\times10^3$

Table 3.

	November	December	January	February	March	April
ERA40	**-0.13**	**-0.38**	**-0.40**	**-0.41**	**-0.33**	**-0.30**
MME	**+0.006**	**+0.016**	**-0.020**	**+0.004**	**-0.003**	**-0.011**
CCCMA-T45	+0.054	+0.070	+0.011	-0.011	-0.002	-0.038
CCCMA-T63	-0.016	+0.026	+0.010	+0.002	+0.038	+0.024
CNRM-CM3	+0.030	+0.028	-0.075	+0.083	+0.074	-0.043
CSIRO-MK3.0	-0.001	-0.027	-0.059	-0.004	-0.031	-0.057
CSIRO-MK3.5	-0.033	-0.028	+0.000	-0.051	+0.022	+0.013
GFDL-CM2.0	+0.006	+0.007	-0.077	-0.069	-0.026	-0.039
GFDL-CM2.1	-0.013	-0.024	-0.065	-0.010	+0.024	-0.024
GISS-AOM	-0.024	+0.010	-0.005	-0.004	-0.028	-0.014
GISS-EH	-0.012	+0.017	-0.025	+0.029	-0.006	-0.017
GISS-ER	-0.043	-0.042	-0.012	-0.023	-0.009	-0.052
IAP	-0.000	+0.009	-0.043	-0.069	+0.022	+0.010
INM-CM3.0	-0.036	-0.024	+0.016	-0.010	+0.050	+0.051
IPSL-CM4	-0.024	+0.030	+0.023	-0.044	-0.017	+0.019
MIROC-3.2 (hires)	+0.028	-0.030	-0.022	-0.022	-0.074	-0.064
MIROC-3.2 (medres)	+0.009	+0.086	+0.022	-0.025	-0.051	-0.004
MPI-ECHAM5	+0.044	+0.043	-0.083	+0.080	-0.043	-0.010
MRI-CGCM2.3.2	+0.037	+0.006	+0.091	+0.033	+0.106	+0.019
NCAR-CCSM3.0	+0.031	+0.069	-0.019	+0.007	-0.007	-0.024
NCAR-PCM1	-0.025	-0.052	-0.074	+0.035	-0.032	-0.018
UKMO-HadCM3	+0.078	+0.071	-0.082	+0.076	-0.000	+0.112
UKMO-HadGEM1	+0.034	+0.104	+0.021	+0.051	-0.062	-0.076